Dynamic Optimization of Human Walking

Frank C. Anderson

Marcus G. Pandy

Department of Biomedical Engineering, and
Department of Kinesiology,
ENS 610,
The University of Texas at Austin,
Austin, TX 78712-D3700

A three-dimensional, neuromusculoskeletal model of the body was combined with dynamic optimization theory to simulate normal walking on level ground. The body was modeled as a 23 degree-of-freedom mechanical linkage, actuated by 54 muscles. The dynamic optimization problem was to calculate the muscle excitation histories, muscle forces, and limb motions subject to minimum metabolic energy expenditure per unit distance traveled. Muscle metabolic energy was calculated by summing five terms: the basal or resting heat, activation heat, maintenance heat, shortening heat, and the mechanical work done by all the muscles in the model. The gait cycle was assumed to be symmetric; that is, the muscle excitations for the right and left legs and the initial and terminal states in the model were assumed to be equal. Importantly, a tracking problem was not solved. Rather, only a set of terminal constraints was placed on the states of the model to enforce repeatability of the gait cycle. Quantitative comparisons of the model predictions with patterns of body-segmental displacements, ground-reaction forces, and muscle activations obtained from experiment show that the simulation reproduces the salient features of normal gait. The simulation results suggest that minimum metabolic energy per unit distance traveled is a valid measure of walking performance. [DOI: 10.1115/1.1392310]

Introduction

Most attempts to quantify *in vivo* muscle forces in humans have combined noninvasive measures of movement with a mathematical theory called optimization. Here, a cost function is hypothesized, and muscle forces are calculated according to the mechanical, energetic, and physiological properties of the neuromusculoskeletal system. Static optimization has been the most common method used to estimate muscle forces during locomotion. This method is computationally inexpensive, and solutions can be obtained relatively quickly on single-processor computers, even when very detailed models of the body are used. Most early static optimization studies included up to 30 muscles per leg [1,2], whereas more recent models have used 42 or more muscles per leg [3,4]. The main disadvantage of static optimization is that the results are heavily influenced by the accuracy of the available experimental data, particularly the measured limb motions [2,5,6].

Dynamic optimization is potentially more powerful than static optimization for two reasons. First, because a time-dependent performance criterion can be posed, the goal of the motor task can be included in the formulation of the problem. Second, dynamic optimization is inherently a forward dynamics method, and so the problem may be formulated independent of experimental data. These two attributes, together, allow the motor patterns and kinematics of movement to be *predicted*. The main disadvantage is that dynamic optimization is computationally very expensive [7,8], so much so that previous solutions for walking have been greatly simplified. The earliest solutions confined the motion of the body to the sagittal plane (e.g., [9]). More recent studies have used muscle-actuated models, but the numbers of muscles included in these models are significantly less than those used in the analogous static optimization work [5,7]. Finally, dynamic optimization simulations of gait have typically been posed as tracking problems, which has compromised the power of this approach as a predictive modeling tool [5,7].

In this paper we present a dynamic optimization solution for normal walking on level ground. Our work is distinguished from previous studies in two respects. First, the model of the body was actuated by a significantly greater number of muscles than has been used in any previous dynamic optimization study (54 muscles total; 24 per leg). Second, the dynamic optimization solution was minimally constrained; we did not solve a tracking problem, but instead used experimental gait data to specify only the initial and final states of the simulation. Our specific aims are: (*a*) to present a physiologically supported, time-dependent, performance criterion for normal walking on level ground; (*b*) to document a method for solving dynamic optimization problems that enables the kinematics and motor patterns for walking to be predicted; and (*c*) to evaluate the model simulation results through comparisons with experimental data.

Methods

Human Experiments. Five healthy adult males participated in this study. The average age, height, and mass of the subjects was 26 ± 3 years, 177 ± 3 cm, and 70.1 ± 7.8 kg, respectively. As a warm-up, each subject walked 4 laps around a 400 m outdoor track. Because the musculoskeletal model used in this study had its arms lumped with the torso and head, each subject was asked to walk with his arms folded across his chest so that the kinematic and kinetic data obtained from the subjects could be compared more directly with the predictions of the model. During the third lap, the number of steps and the time required to complete the lap were measured, from which a step frequency was found. Each subject then practiced walking on an 11 m long, level walkway in the laboratory. A force-plate was mounted flush with the surface of the walkway, with the front edge of the plate lying 8 m from the beginning of the walkway. Step frequency was reproduced in the laboratory by setting a metronome to the subject's measured outdoor step frequency. Each subject marched in place at the beginning of the walkway and began forward progress at a time of his choosing.

Passive reflective markers (2.54 cm and 5.08 cm in diameter) were placed on both the left and right sides of the body to measure the three-dimensional positions of the segments. Pairs of preamplified EMG surface electrodes (Iomed Inc., Salt Lake City, UT) were attached to the right leg and torso to record activity in 11 muscles: tibialis anterior, soleus, lateral gastrocnemius, vastus lateralis, rectus femoris, hamstrings, adductor magnus, gluteus maximus, gluteus medius, erector spinae, and the external abdominal obliques.

Contributed by the Bioengineering Division for publication in the JOURNAL OF BIOMECHANICAL ENGINEERING. Manuscript received by the Bioengineering Division October 21, 1999; revised manuscript received May 16, 2001. Associate Editor: M. L. Hull.

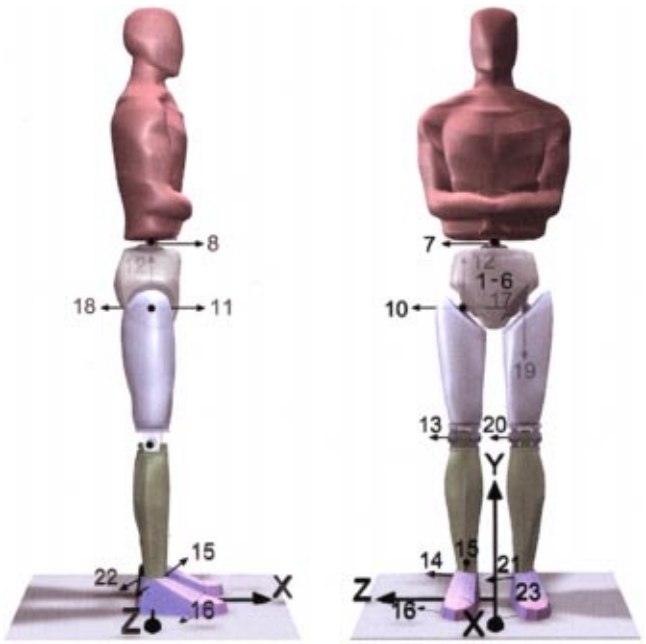

Fig. 1 Sagittal- and frontal-plane views of the model skeleton. The inertial reference frame was fixed to the ground at the level of the floor. The axes of the inertial frame formed a right-handed coordinate system: The X axis was directed forward, the Y axis was directed upward, and the Z axis was directed laterally. There were a total of 23 generalized coordinates in the model. Wherever possible, each generalized coordinate is labeled as a number. Generalized coordinates q_1-q_3 specified the translation of the pelvis with respect to the origin of the inertial frame, and q_4-q_6 were *X-Y-Z* body-fixed, Euler angles which specified the orientation of the pelvis with respect to the inertial frame. The relative orientations of the HAT, right thigh, and left thigh with respect to the pelvis were specified using *Z-X-Y* body-fixed Euler angles at the back (q_7-q_9), right hip ($q_{10}-q_{12}$), and left hip ($q_{17}-q_{19}$), respectively. Generalized coordinate q_9 (rotation of the HAT in the transverse plane) is not shown because it lies inside the HAT segment.

Five trials were collected for each subject, with video, force-plate, and EMG data recorded simultaneously during each trial. Data collection was triggered by a photosensitive eye. Kinematic data were recorded using a four-camera, video-based system (Motion Analysis Inc., Santa Rosa, CA). Marker positions were low-pass filtered using an order 20 finite impulse response (FIR) filter with a cutoff frequency of 6 Hz. Joint angles were calculated from the three-dimensional marker coordinates using the methods described by Anderson [10]. Ground-reaction forces and moments were measured using a six-component, strain-gauge force plate (Bertec Inc., Columbus, OH). All channels from the force plate were sampled at 1000 Hz, as were the analog EMG data. EMG data were band-pass filtered between 50 and 200 Hz using an order 100 FIR filter, and these data were then rectified.

Musculoskeletal Model of the Body. The model has been described in detail by Anderson and Pandy [11], and only a brief description is given here. The skeleton was represented as a 10 segment, 23 degree-of-freedom (dof) mechanical linkage (Fig. 1). The pelvis was modeled as a single rigid body with 6 dof; the remaining 9 segments branched in an open chain from the pelvis. The head, arms, and torso (HAT) were lumped into a single rigid body, and this segment articulated with the pelvis via a 3 dof ball-and-socket joint located at the third lumbar vertebra. Each hip was modeled as a 3 dof ball-and-socket joint, and each knee was modeled as a 1 dof hinge. Two segments were used to model each foot: a hindfoot segment and a toes segment. The hindfoot articulated with the tibia via a 2 dof universal joint comprising two axes of rotation: one for the ankle and the other for the subtalar joint. The toes articulated with the hindfoot via a 1 dof hinge joint. Details relating to the axes and centers of rotation of the joints are given by Anderson [10].

Anthropometric measurements were taken for each subject following the procedures described by McConville et al. [12]. The model anthropometry was set to the average of the subject measures [10]. The dynamical equations of motion for the model skeleton were obtained in symbolic form using a software package called SD/Fast (Symbolic Dynamics Inc., Mountain View, CA).

The interaction of the feet with the ground was simulated using a series of spring-damper units distributed under the sole of each foot. Four ground springs were located at the corners of the hindfoot segment, and one was positioned at the distal end of the toes. Each ground spring applied forces in the vertical, fore-aft, and transverse directions simultaneously. The force acting in the vertical direction varied exponentially with the height of the foot above the ground, while those applied in the fore-aft and transverse directions varied linearly with the displacement of the foot in each of these directions [11].

The model was actuated by 54 musculotendon units. Each leg was actuated by 24 muscles, and relative movements of the pelvis and HAT were controlled by 6 abdominal and back muscles (Fig. 2). The path of each musculotendon actuator was based on geometric data (musculotendon origin and insertion sites) reported by Delp [13]. Wherever possible, each muscle group was represented by a single actuator; for example, biceps femoris long head, semimembranosus, and semitendinosus were combined into hamstrings. Gluteus maximus and gluteus medius/minimus, because they have fanlike origins on the pelvis, were each separated into two actuators. When an actuator wrapped around bone or other muscles, via points and via cylinders were used to represent its path more precisely [14].

Each actuator was modeled as a 3-element, Hill-type muscle in series with an elastic tendon [15]. Parameters defining the nominal properties of each actuator (i.e., peak isometric force and the corresponding fiber length and pennation angle of muscle plus tendon slack length) were based on data reported by Delp [13]. The maximum shortening velocity of each muscle in the model was taken to be 10 optimal muscle fiber lengths per second, which assumes that all muscles in the body have mixed fiber types [15]. Values of peak isometric muscle force and tendon slack length were adjusted so that the maximum isometric torque-angle curves for each joint in the model matched average torque-angle curves measured for the five subjects. Values of the musculotendon parameters assumed for each actuator in the model are given in Table 3 of Anderson and Pandy [11].

Muscle excitation–contraction dynamics were modeled using a first-order differential equation to relate the rate of change in activation to the muscle excitation signal [15]. In the model, the activation level of a muscle was allowed to vary continuously between zero (no contraction) and one (full contraction). The muscle excitation signal was assumed to represent the net effect of both motorneuron recruitment and stimulation frequency, and was also allowed to vary continuously between zero (no excitation) and one (full excitation). The rise and decay time constants for muscle activation were assumed to be 22 and 200 ms, respectively [15]. The general forms of the equations used to model excitation-contraction dynamics, musculotendon dynamics, and skeletal dynamics are given by Anderson and Pandy [11].

Performance Criterion. It has been observed that people walk at speeds which correspond to a minimum metabolic energy cost per unit distance traveled (Fig. 3) [16]. Based on this result, we hypothesized that the motor patterns that typify normal gait are the result of a minimization in metabolic energy expenditure per unit distance moved. The performance criterion for the dynamic optimization problem was therefore expressed as follows:

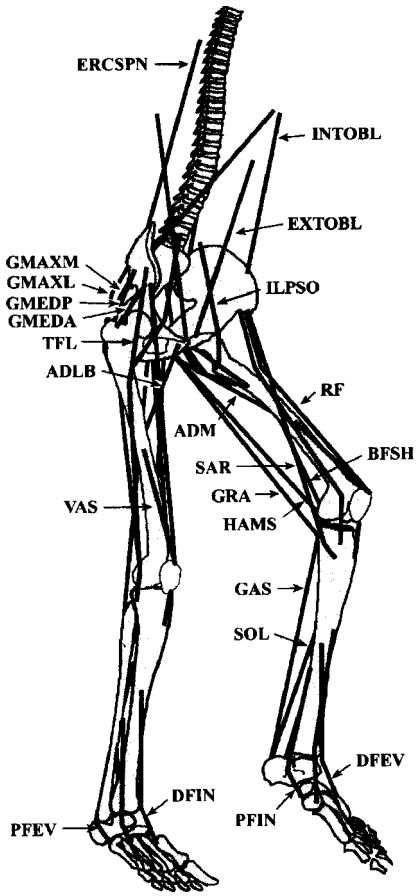

Fig. 2 Schematic showing some of the muscles in the model. A total of 54 musculotendinous actuators controlled the model. Abbreviations used for the muscles are as follows: ERCSPN, erector spinae; EXTOBL, external abdominal obliques; INTOBL, internal abdominal obliques; ILPSO, iliopsoas; ADLB, adductor longus brevis; ADM, adductor magnus; GMEDA, anterior gluteus medius and anterior gluteus minimus; GMEDP, posterior gluteus medius and posterior gluteus minimus; GMAXM, medial gluteus maximus; GMAXL, lateral gluteus maximus; TFL, tensor fasciae latae; SAR, sartorius; GRA, gracilis; HAMS, semimembranosus, semitendinosus, and biceps femoris long head; RF, rectus femoris; VAS, vastus medialis, vastus intermedius, and vastus lateralis; BFSH, biceps femoris short head; GAS, gastrocnemius; SOL, soleus; PFEV, peroneus brevis and peroneus longus; DFEV, peroneus tertius and extensor digitorum; DFIN, tibialis anterior and extensor hallucis longus; PFIN, tibialis posterior, flexor digitorum longus, and flexor hallucis longus. Muscles included in the model but not shown in the diagram are: PIRI, piriformis; PECT, pectinius; FDH, flexor digitorum longus/brevis and flexor hallucis longus/brevis; and EDH, extensor digitorum longus/brevis and extensor hallucis longus/brevis.

$$E_d = \frac{\int_0^{t_f} \dot{E}^M_{\text{total}}}{X_{cm}(t_f) - X_{cm}(0)} = \frac{\int_0^{t_f} \left(\dot{B} + \sum_{m=0}^{54} (\dot{A}_m + \dot{M}_m + \dot{S}_m + \dot{W}_m) \right) dt}{X_{cm}(t_f) - X_{cm}(0)}, \quad (1)$$

where $\dot{E}^M_{\text{total}}$ is the rate at which total metabolic energy is consumed in the model, and $X_{cm}(0)$ and $X_{cm}(t_f)$ denote the position of the center of mass of the model at the initial and final times of the simulated gait cycle. $\dot{E}^M_{\text{total}}$ was computed by adding the basal metabolic heat rate of the whole body ($\dot{B}$) to the activation heat rate ($\dot{A}_m$), maintenance heat rate ($\dot{M}_m$), shortening heat rate ($\dot{S}_m$), and the mechanical work rate ($\dot{W}_m$) of each muscle m in the model. The equations used to estimate metabolic energy from the internal states of the muscles were developed based largely on the work of Davy and Audu [5], Hatze and Buys [17], and Mommaerts [18]. Details of our model of muscle energy production are given by Anderson [10].

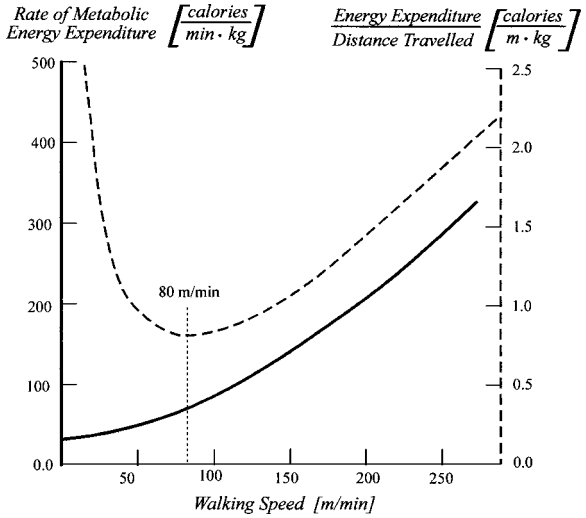

Fig. 3 Metabolic energy expenditure plotted as a function of walking speed. The rate of metabolic energy expenditure increases parabolically as walking speed increases (solid line) [16]. When the rate of metabolic energy consumption is normalized by the distance traveled, an optimal walking speed is predicted at 80 m/min (dashed line) [16].

To limit hyperextension of the joints, a penalty function, ϕ, was appended to the performance criterion,

$$\phi = w \int_0^{t_f} \left[\sum_{j=1}^{17} T^2_{lig_j} \right] dt, \quad (2)$$

where $w(0.001)$ is a parameter that weights the value of the penalty function against the value of the performance criterion, and T_{lig_j} is the torque applied by the ligaments at the jth joint. Ligament torques varied exponentially with angular displacement and linearly with angular velocity of the joints (see [11] for details). $j = 1,17$ in Eq. (2) because ligament torques are applied only at the rotational joints of the model.

Constraints. To reduce computations, a full gait cycle was reconstructed by simulating one half of a gait cycle and assuming bilateral symmetry. That is, it was assumed that the left-side stance and swing phases were the mirror of the right-side stance and swing phases, respectively. The final time of the simulation was fixed at 0.56 s, which corresponds to the average time for half a cycle measured for the subjects.

Only a set of terminal constraints was specified in the optimization problem, and this was done in order to enforce repeatability of the gait cycle. Specifically, the values of the joint-angular displacements, joint-angular velocities, muscle forces, and muscle activations at the end of the simulation were required to be the same as the values at the beginning. Because only half a cycle was simulated, symmetry required that the final states of the right side of the body be equal to the initial states of the left side of the body, and *vice versa*. However, this principle could not be applied to the orientation of the pelvis or HAT, because there is no left or right side joint for these two bodies. Instead, for the pelvis and

HAT, symmetry required that the joint-angular displacements and velocities alternate sign about the x and y axes of these bodies, and that these variables retain the same sign about the z axis (see Fig. 1 for a definition of the joint axes). No constraints were placed on the position of the center of mass of the pelvis, nor was it necessary to place constraints on either of the metatarsal joints. Altogether, 18 terminal constraints were placed on the joint-angular displacements and another 18 on the joint-angular velocities (e.g., 23 total generalized coordinates minus 3 coordinates for the translation of the pelvis minus 2 coordinates for the angles of the two metatarsals). Note that this formulation meant that a tracking problem was not solved; that is, between $t=0$ and $t=0.56$ s, the joint angles and joint-angular velocities were free to take any values dictated by the dynamics of the system.

For each muscle in the model, one terminal constraint was imposed to enforce continuity of the muscle activations and muscle forces. Specifically, the activation of each muscle on the right side of the body at the end of the simulation was constrained to equal the activation of the corresponding muscle on the left side of the body at the beginning of the simulation, and *vice versa*. It was unnecessary to explicitly enforce continuity of the muscle forces, because this condition is guaranteed once the muscle activations, joint-angular velocities, and joint-angular displacements are all continuous. Again, note that between $t=0$ and $t=0.56$ s, the values of the muscle activations and muscle forces were free to accept any values determined by the dynamics of the system.

Initial States. The simulation began at left toe-off and ended at right toe-off. The initial values of all the generalized coordinates in the model, except the vertical displacement of the pelvis, pelvic tilt, and the subtalar joint angle, were based on average values measured for the five subjects at left toe-off. Because the vertical displacement of the pelvis, pelvic tilt, and subtalar joint angle could not be determined accurately enough from the subjects' gait data, the values of these variables were calculated so that the vertical ground reaction force at left toe-off in the model approximated the average value measured at the same instant for the subjects. The initial values of the muscle activations also could not be determined from the gait data, so these variables were specified as additional controls in the problem. Once an initial guess was made for the initial muscle activations, the corresponding initial values of the muscle forces were computed based on the force-length-velocity properties of muscle and the initial muscle activations, joint-angular velocities, and joint-angular displacements. A detailed description of the methods used to specify the initial states of the model is given by Anderson [10].

Dynamic Optimization Problem. The problem was to minimize Eq. (1) subject to the dynamical equations of motion of the model, the penalty function which accounts for action of the ligaments in limiting joint hyperextension (Eq. (2)), and the constraints imposed at the beginning and end of the simulated gait cycle.

Computational Solution. The dynamic optimization problem was solved using parameter optimization [8,19]. The excitation histories for all the muscles were the inputs to the model. Each excitation history was discretized into a set of independent variables called control nodes. The problem was then to find the values of the control nodes which minimized the performance criterion (Eq. (1)). Fifteen control nodes, each separated by 37.3 ms, were used to represent the time-history of each muscle excitation. In addition, because the initial muscle activations were unknown, these variables also appeared as control variables in the parameter optimization problem.

Constraining the simulated gait cycle to repeat requires that the muscle excitation histories be continuous. This condition was enforced for each muscle in the model by making the value of the last control node for the right side of the body equal to the value of the first control node for the body's left side. Thus, the total number of control variables optimized was 810: 54 muscles$\times$15 nodes/muscle$-$54$+$54. Fifty-four nodes were subtracted because the last control node for each muscle was constrained to have the same value as the first node; 54 nodes were added because the initial values of all the muscle activations were free. Computations were performed initially on an IBM SP-2 and were completed on a Cray T3E.

Results

Kinematics. The model and the subjects walked at an average speed of 81 m/min, which is very close to the optimal speed estimated by Ralston [16]. In addition, for most of the gait cycle, the majority of joint angular displacements predicted by the model were within one standard deviation of the joint angular displacements measured for the subjects. The model pelvis oscillated with amplitudes of about 5 deg in both the frontal and sagittal planes (cf. black and gray lines for List and Tilt in Fig. 4). The back joint

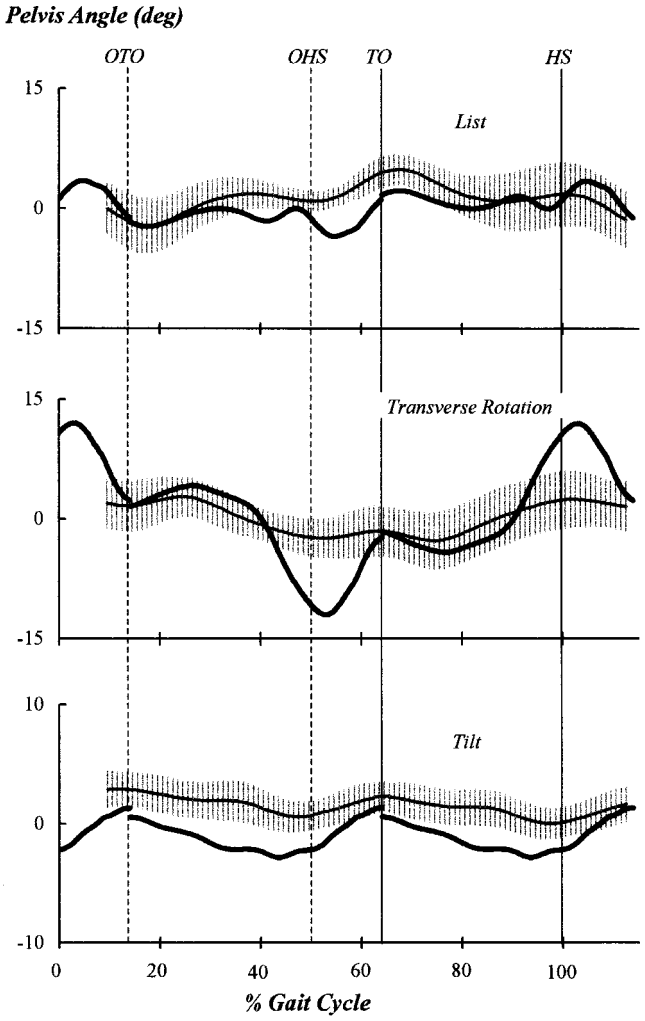

Fig. 4 Orientation of the pelvis in the model (black lines) and in the subjects (gray lines). The gray vertical lines represent one standard deviation above and below the mean for the subjects. 0 and 100 percent indicate heel strike of the same leg (one gait cycle) for the model and the subjects. The orientation of the pelvis is described by the body-fixed *X-Y-Z* Euler angles (see Fig. 1). Pelvic list (top) occurs about the *X* axis of the pelvis, with listing to the right being positive. Transverse rotation (middle) occurs about the *Y* axis of the pelvis, with rotation to the left being positive. Pelvic tilt (bottom) occurs about the *Z* axis of the pelvis, with posterior tilt being positive. OTO denotes opposite toe-off, OHS opposite heel-strike, TO toe-off, and HS heel strike.

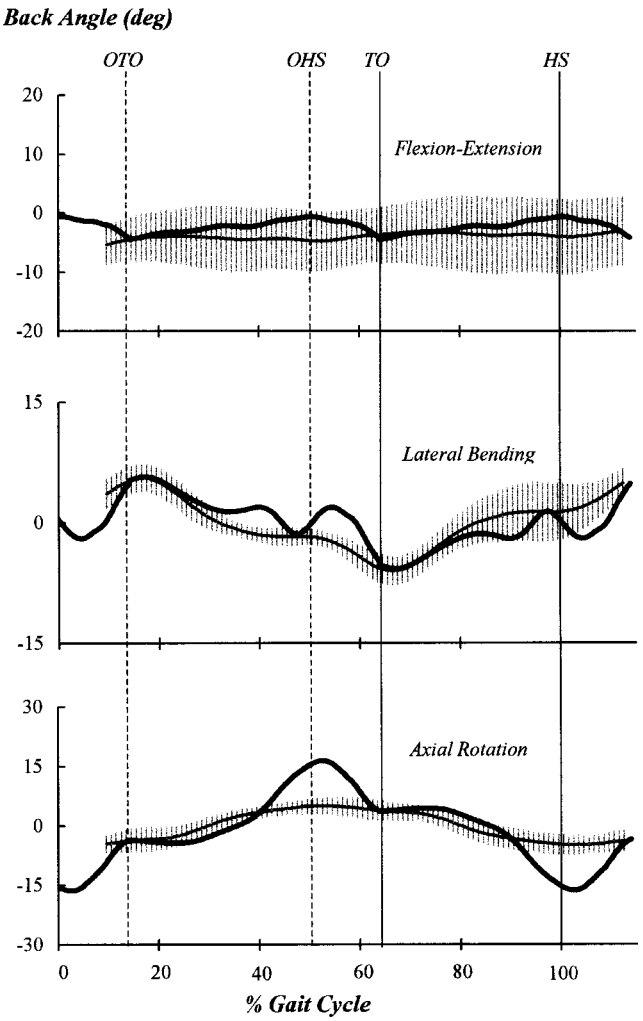

Fig. 5 Angular displacement of the back in the model (black lines) and in the subjects (gray lines). The gray vertical lines represent one standard deviation above and below the mean for the subjects. The back angles define the orientation of the HAT segment relative to the pelvis and are described by body-fixed *Z-X-Y* Euler angles (Fig. 1). Flexion-Extension (top) occurs about the *Z* axis of the HAT, with extension being positive. Lateral Bending (middle) occurs about the *X* axis of the HAT, with bending to the right being positive. Axial Rotation (bottom) occurs about the *Y* axis of the HAT, with rotation to the left being positive.

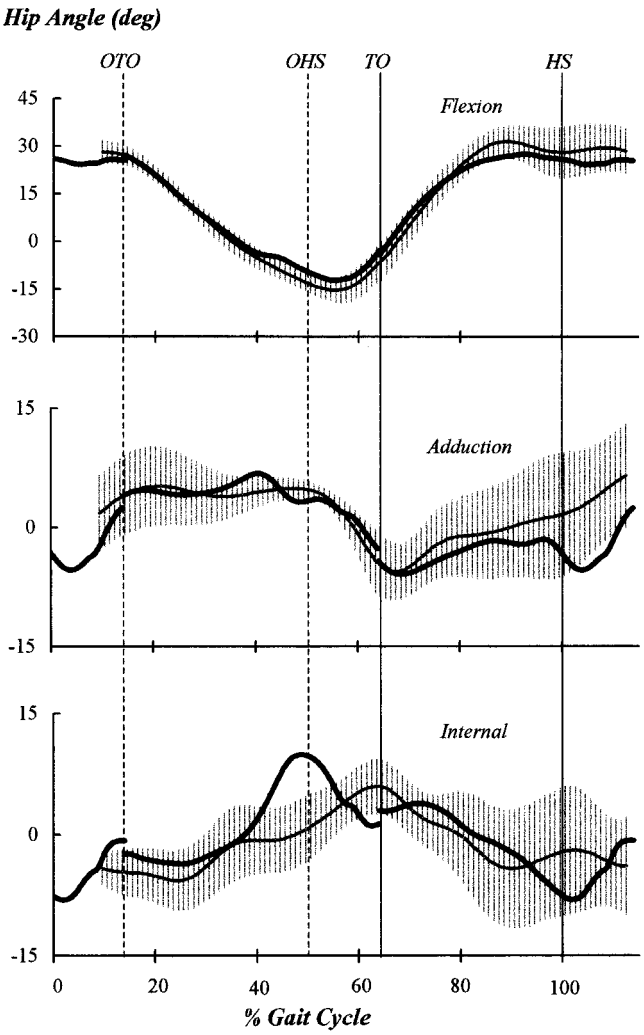

Fig. 6 Angular displacement of the hip in the model (black lines) and in the subjects (gray lines). The gray vertical lines represent one standard deviation above and below the mean for the subjects. The hip angles define the orientation of the thigh relative to the pelvis and are described by body-fixed *Z-X-Y* Euler angles (Fig. 1). Flexion-extension (top) occurs about the *Z* axis of the thigh, with flexion being positive. Abduction-adduction (middle) occurs about the *X* axis of the thigh, with adduction being positive. Internal-external rotation (bottom) occurs about the *Y* axis of the thigh, with internal rotation being positive.

angles oscillated with amplitudes of approximately 5 deg about the anatomical position (black and gray lines in Fig. 5). Hip flexion angles in the model and subjects were very similar until about 80 percent of the cycle, after which time the model did not use quite as much hip flexion as the subjects (Fig. 6, compare black and gray lines for Flexion between 80 and 100 percent). In the frontal plane, the hip adducted and abducted about 5 deg during stance and swing (cf. black and gray lines for Adduction in Fig. 6). Following heel strike, the knee flexed 20 deg until opposite toe-off, extended to near full extension prior to opposite heel strike, flexed to 70 deg shortly after toe-off, and then extended again to near full extension at heel strike (black line for Knee Extension in Fig. 7). During stance, the ankle dorsiflexed and then plantarflexed rapidly in preparation for toe-off, while the subtalar joint was fixed at -7 deg (black lines for Ankle Dorsiflexion and Subtalar Inversion in Fig. 7 from OTO to OHS). Just before opposite heel strike, as the heel of the stance foot left the ground, the subtalar joint inverted by about 15 deg (black and gray lines for Subtalar Inversion near OHS).

The largest discrepancies between the predicted and measured joint angular displacements occurred in the transverse plane (Transverse Rotation in Fig. 4, Axial Rotation in Fig. 5, and Internal in Fig. 6 at approximately 50 percent). In particular, the pelvis in the model was rotated by as much as 12 deg in the transverse plane, compared to only 5 deg in the subjects (Fig. 4, compare black and gray lines near HS for Transverse Rotation). There were other smaller, but notable, discrepancies. The model tilted its pelvis slightly more anterior than did the subjects. This difference could simply have been due to a small error in registering the model and subject pelvic coordinate frames (Tilt in Fig. 4). Also, the model did not extend its knee as fully as the subjects, and it dorsiflexed its ankle considerably more than the subjects toward the end of single support (Knee Extension and Ankle Dorsiflexion in Fig. 7 from 40 to 50 percent). We believe this underextension of the knee and exaggerated dorsiflexion of ankle in the model are related to each other and reflect a tendency of the op-

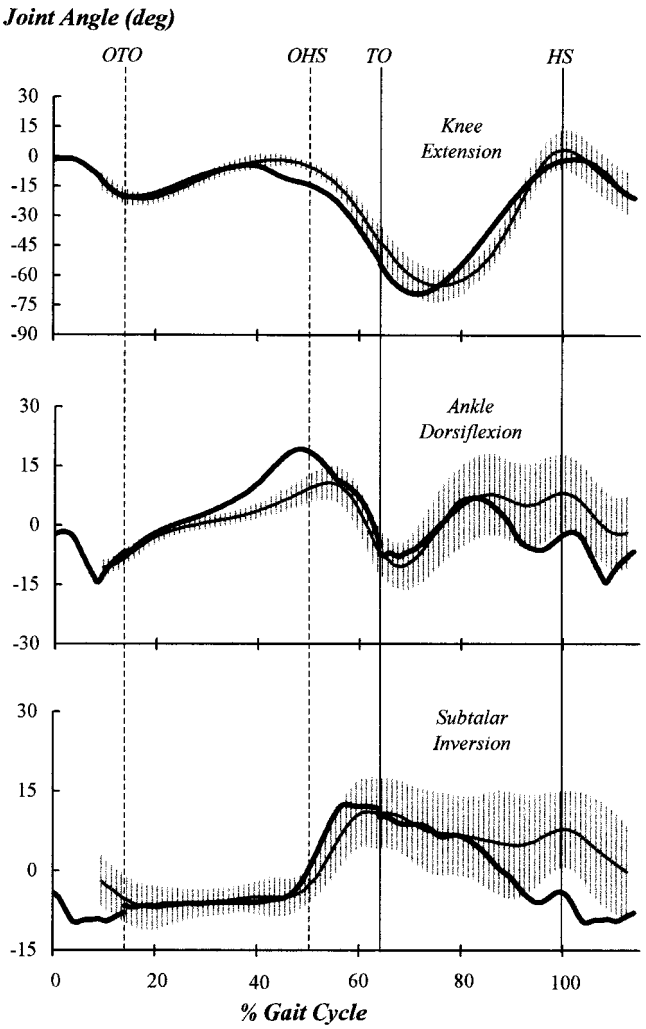

Fig. 7 Angular displacements of the knee, ankle, and subtalar joints in the model (black lines) and in the subjects (gray lines). The gray vertical lines represent one standard deviation above and below the mean for the subjects. Knee extension, ankle dorsiflexion, and subtalar inversion are all positive.

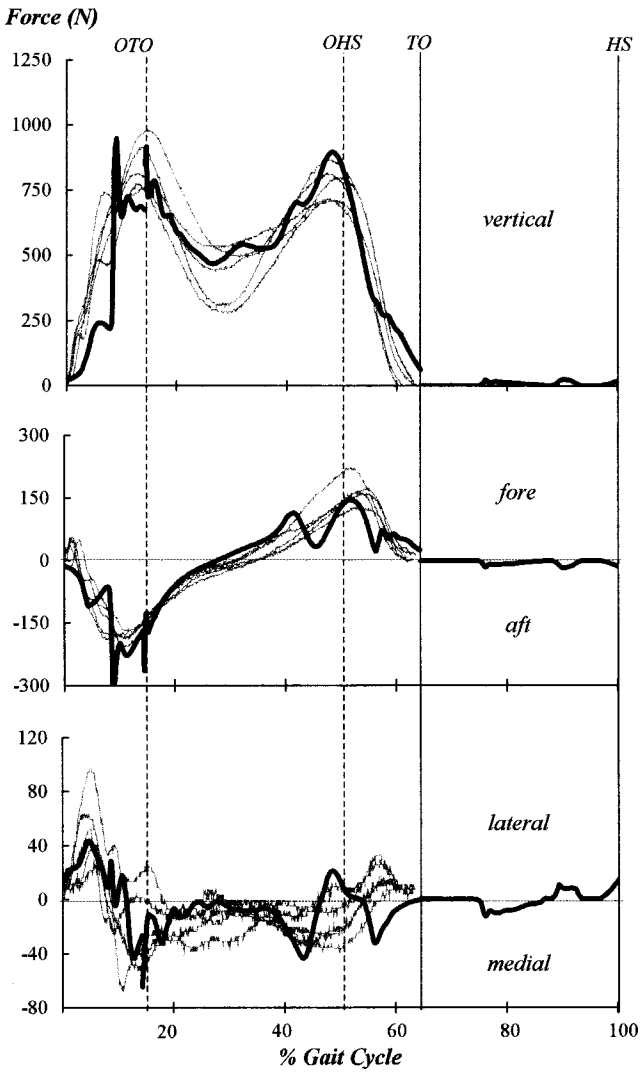

Fig. 8 Vertical, fore-aft, and transverse components of the ground-reaction force generated by the model (black lines) and the subjects (gray lines) during walking. For the model, the resultant force in each direction was found by summing the forces developed by the ground springs located under the sole of each foot. Spikes in the model ground forces are due to oscillations in the ground springs.

timization solution to avoid hyperextending the knee and incurring performance penalties (see Eq. (2)).

Ground-Reaction Forces. The vertical force exerted by the ground showed the familiar double-hump pattern, with the first hump occurring near opposite toe-off and the second hump occurring just prior to opposite heel strike (black and gray lines for Vertical in Fig. 8). Consistent with force records obtained for two of the subjects, the vertical ground force for the model showed a small peak shortly after heel strike. The fore-aft component was directed posteriorly from heel strike to 30 percent of the cycle, and anteriorly thereafter (cf. black and gray lines for Fore-Aft). The variation in the mediolateral component was more complicated, but the result predicted by the model was very similar to that measured for the subjects until 40 percent of cycle time (cf. black and gray lines for Lateral-Medial).

One of the more notable differences between model and experiment relates to the fore-aft component of the ground-reaction force. The model produced three separate peaks in the fore-aft component of the ground force near opposite heel strike, whereas the subjects generated a more uniform distribution of force in this direction (cf. black and gray lines for Fore-Aft near OHS in Fig. 8). Another, more minor, anomaly in the model was the nonzero ground force produced during swing. This result was brought about by the toe and heel of the model brushing the ground very lightly as the leg was swung through (black lines at 75 and 90 percent of cycle time in Fig. 8).

Muscle Excitation Patterns. The muscle excitation histories predicted by the model were, for the most part, consistent with EMG measured for the subjects and with EMG data reported by others (Fig. 9, compare black lines with wavy gray lines and horizontal gray bars). The back muscles were quiet throughout the gait cycle, except in the neighborhood of opposite heel strike. Subjects showed a pronounced burst of activity in their erector spinae, a behavior that was reproduced in the model, but at slightly later times (cf. black lines with gray wavy lines and gray bars around OHS for ERCSPN). The medial and lateral portions of gluteus maximus were excited mainly during double support (Fig. 9, GMAXM and GMAXL). The abductors were excited in a double burst: the first occurring during double support, and the second during the middle portion of single support (cf. black lines with gray wavy lines and gray bars for GMEDP and GMEDA). Iliopsoas in the model and the subjects was excited from just prior to

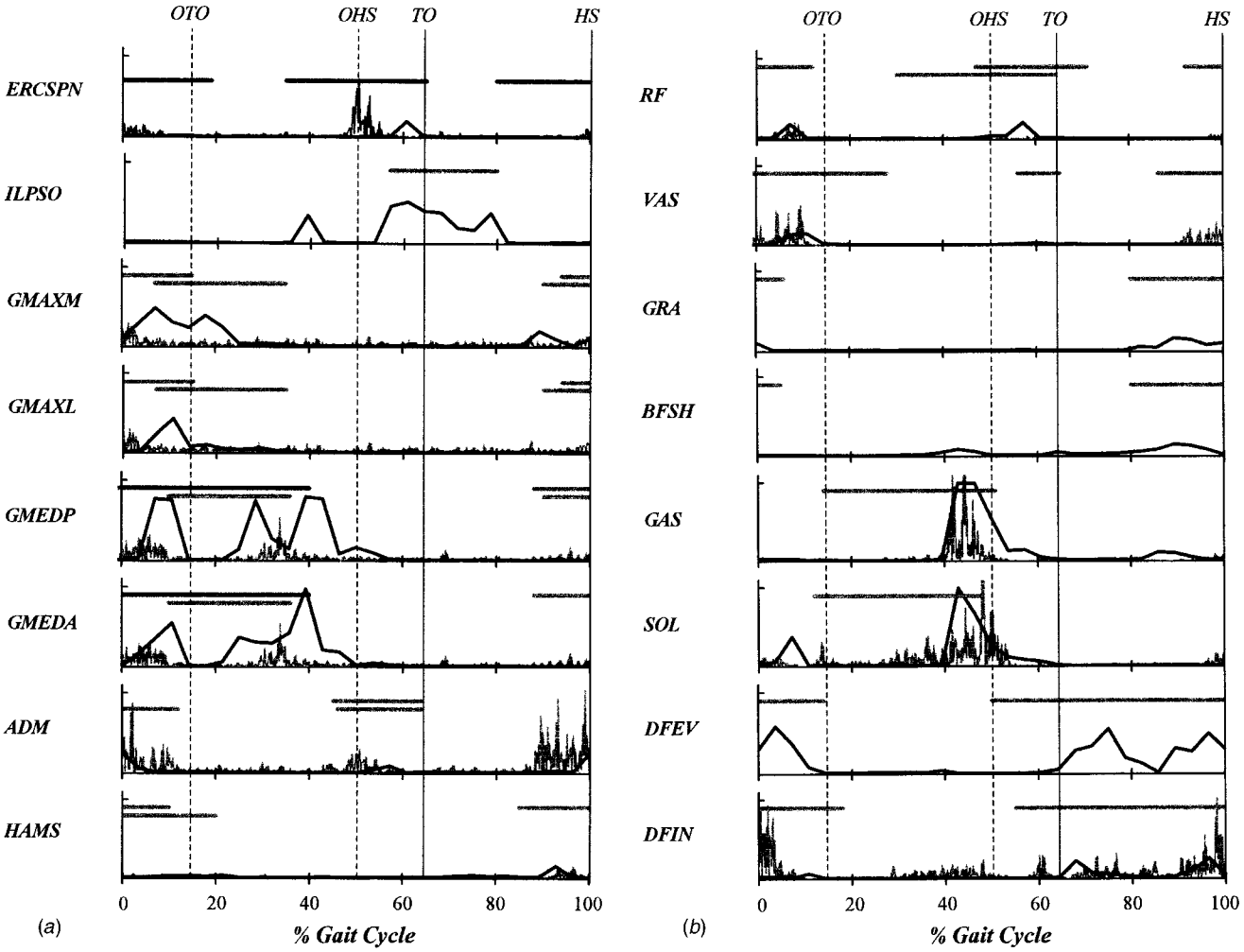

Fig. 9 Comparison of EMG data recorded for one subject (gray wavy lines) with muscle excitation histories predicted by the model (black lines) for walking. Subject EMG data were normalized by dividing by the maximum electrode voltage recorded during a maximal voluntary contraction for each muscle. The vertical axes for the model excitations and subject EMG records therefore range from 0 to 1. The horizontal gray bars shown above many of the records indicate the periods of EMG activity recorded by other researchers [28,29]. 0 and 100 percent indicate heel strike of the same leg (one gait cycle) for the model and the subjects. Abbreviations used for the muscles are given in Fig. 2.

toe-off up to the middle portion of swing. In contrast to experiment, the model also predicted a short burst of iliopsoas activity at 40 percent of cycle time (cf. black line with gray bar for ILPSO).

Consistent with experiment, the model vasti and rectus femoris were excited simultaneously between heel strike and opposite toe-off and between opposite heel strike and toe-off (cf. black lines with wavy gray lines and gray bars for VAS and RF in Fig. 9). Subjects also activated their vastus muscles prior to heel strike, but vasti in the model remained silent at this time (gray wavy lines and gray bars for VAS near HS). The solution predicted co-contraction of the biarticular hamstrings with rectus femoris and vasti. These predictions of the model are consistent with the muscle coordination patterns utilized by people, and they lend support to a minimum-metabolic-energy hypothesis for normal walking.

Similar levels of agreement between model and experiment were obtained for the muscles crossing the ankle and metatarsal joints. Soleus and gastrocnemius were fully excited just prior to opposite heel strike, a behavior characteristic of the push-off phase of gait. However, the model also predicted activity in gastrocnemius just prior to heel strike, and in soleus just prior to opposite toe-off. Although these results are not confirmed by EMG data available from other studies, there is evidence of small-amplitude activity in gastrocnemius and soleus in the EMG data recorded from our subjects (Fig. 9, gray wavy lines near HS for GAS and near OTO for SOL). In agreement with the experimental results, the model dorsiflexors were excited during double support and during the ensuing swing phase as well (cf. black lines with wavy gray lines and gray bars for DFEV and DFIN).

Table 1 Muscle metabolic energy consumption predicted by the dynamic optimization solution for walking. One-half of the gait cycle was simulated, so all calculations of energy production were multiplied by a factor of 2 to give results for a full cycle. During one cycle, the center of mass of the model moved forward a distance of 1.52 meters in 1.12 s. Thus, forward walking velocity of the model was 1.36 m/s or 81.6 m/min. Total mass of the model was 71.005 kg.

Units	Mechanical work	Maintenance heat	Basal heat	Activation heat	Shortening heat	Total
J	166	122	120	77	42	527
J/s	148	109	107	70	38	472
J/m	109	80	79	50	27	345
J/kg·m	1.5	1.1	1.1	0.7	0.4	4.8
J/kg·s	2.1	1.5	1.5	1.0	0.5	6.6

Metabolic Cost. The model expended metabolic energy at a rate of 6.6 J/(kg·s), which is a good deal higher than the value of 4.5 J/(kg·s) obtained from oxygen consumption measurements made in people [20]. Ranked in order of decreasing magnitude, the separate contributions to total metabolic cost were: mechanical work, maintenance heat, basal heat, activation heat, and shortening heat (Table 1). These results suggest that the mechanical efficiency of muscles for normal walking is about 30 percent, which is a little lower than the value obtained from heat measurements made on isolated muscle preparations [21].

Discussion

Several aspects of this work should be contrasted with previous dynamic optimization studies. First, we hypothesized that the motor patterns that typify walking at normal speeds are adopted in order to effect an efficient conversion of metabolic energy into translation and rotation of the body segments. The criterion used to quantify this hypothesis was minimum metabolic energy consumed per unit distance traveled. Although the results of many experimental studies support this criterion as a measure of walking performance, it has not been used previously to solve a dynamic optimization problem for gait. In their three-dimensional simulation of walking, Yamaguchi and Zajac [7] minimized differences between model and experimental joint trajectories without accounting for the physiological cost of movement. Davy and Audu [5] did account for the amount of metabolic energy consumed by muscles during the swing phase of gait, but metabolic energy was *not* normalized by the distance moved. Normalizing metabolic energy by the distance traveled is especially important to the dynamic optimization problem formulated here because, as Ralston [16] has shown, metabolic energy increases monotonically with speed, and a minimum is obtained only when the rate of metabolic energy consumption is divided by walking speed.

Second, a significant feature of the problem solved in this study is the fact that the body motions, ground-reaction forces, and muscle excitation patterns were all *predicted*, not prescribed by experimental data. Previous studies have solved dynamic optimization problems for gait by forcing the model to track measurements of the time histories of body-segmental displacements and velocities. In this study, all the body-segmental motions, ground-reaction forces, muscle activations, and muscle excitation histories in the model were predicted given only the states of the model (i.e., the positions and velocities of all the body segments) at the beginning and end of the gait cycle. The fact that the predicted kinematics, ground-reaction forces, and muscle coordination patterns are similar to those obtained from experiment supports the use of minimum metabolic energy per unit distance traveled as a measure of walking performance.

Third, our three-dimensional simulation of walking is much more elaborate than what has been published previously. We modeled the body as a 23-dof mechanical linkage actuated by 54 leg, abdomen, and back muscles. This increase in overall model complexity was necessary to predict the motions of the various body segments outside of the sagittal plane. In particular, ball-and-socket joints were needed to represent the back joint and both hip joints in order to allow the pelvis to list in the frontal plane and to externally and internally rotate in the transverse plane. These rotations are important for flattening and smoothing the motion of the center of mass during walking [22]. In addition, inclusion of subtalar joints in the model was needed to allow the center of mass to move laterally over the stance leg during support. A large number of muscles (more than 50) was needed to effect an appropriate level of control over these degrees of freedom. The number of muscles, in particular, is two to six times greater than that considered in previous dynamic optimization solutions for walking. Finally, a relatively detailed model of the foot was needed to accurately and efficiently simulate impact of the feet with the ground.

Fourth, the model used in this study is suitable for investigating a range of activities, not just walking. The model has been used to solve a dynamic optimization problem for maximum-height jumping [11], and we believe that it could also be used to simulate stair climbing, rising from a chair, and running. One of the great difficulties in modeling any biological system is estimating the values of its parameters. By simulating different activities, different aspects of the model are tested, which then allow for deeper refinement of the model parameters. For example, by solving a dynamic optimization problem for maximum-height jumping, a task that presents a well-defined performance criterion and also demands large forces from many of the extensor muscles, we were able to make necessary adjustments to the strengths of the trunk muscles, which would otherwise have gone unnoticed had we only simulated walking.

Differences between the model predictions and experimental data are evident, however, and these differences are explained by the limitations of the model. The most conspicuous discrepancy in the response of the model concerns the motion of the pelvis in the transverse plane. There was an exaggerated transverse rotation of the pelvis near heel strike, which was also visible in the kinematics of the back and hip joints (black lines in Figs. 4, 5, and 6 near HS and OHS). This anomaly in the model is due to the forces needed to decelerate the swing leg in preparation for opposite heel strike. Specifically, the swing leg pulled the swing-side pelvis forward in the model, as the swing leg's forward progression was slowed prior to heel strike. This behavior was not demonstrated by the subjects possibly because the mechanisms for controlling the motion of the pelvis are much more intricate in the human than in the model. The model may have lacked important external rotators at the hip. In addition, the pelvis and HAT segments in the model were separated only by a 3 dof back joint controlled by 6 muscles, whereas the individual vertebrae of the spine rotate on each other in the transverse plane and are controlled by perhaps as many as 50 muscles during gait.

Many of the remaining differences between model and experiment are likely due to the model of the foot. Spikes in the vertical ground-reaction force just prior to opposite toe-off are caused by very small-amplitude oscillations in the foot springs. The vertical force also does not fall to zero at the end of the stance phase in the model, which results from a delay in weight transfer onto the contralateral leg at the beginning of double support. This behavior is clearly evident at heel strike, where the vertical force calculated in the model lags behind the force records obtained for the subjects (cf. black and gray lines between 0 and 10 percent for Vertical in Fig. 8). The three separate peaks in the fore-aft component of the ground force between 45 and 55 percent of the cycle are caused by the damping elements in the foot springs, as first the heel and then the toes leave the ground. Modeling the sole of the foot more accurately may have allowed the foot to roll just after heel strike and during push-off. Anticipated effects of this change in the model are improved joint kinematics at the knee and ankle, improved muscle-force histories for the ankle plantarflexors, and more accurate vertical and fore-aft components of the ground-reaction force.

The computed solution also did not meet the terminal constraints specified in the dynamic optimization problem for gait. Small discontinuities can be seen in the orientation of the pelvis, in the joint angles for the back, hip, knee, and ankle (black lines in Figs. 4, 5, 6, and 7), and in all three components of the ground-reaction force (black lines in Fig. 8). These differences are the accumulated effect of small differences between the joint-angular displacements and joint-angular velocities of the ankle, knee, hip, back, and pelvis for the model and the subjects. Failure to meet the terminal constraints is due to the large size and the high nonlinearity of the optimization problem solved. Given enough computation time, our optimization algorithm would likely converge to a point where the terminal constraints were met with arbitrary tolerance; however, after computing the solution for almost

10,000 hours of CPU time, the benefit of continuing the computation was no longer justified by the cost in computer time. (Note that 10,000 hours of CPU time translates to much less wall-clock time because the problem was solved in parallel using as many as 32 processors at a time.)

Finally, the model consumed metabolic energy at a much higher rate (almost 50 percent) than that measured for people walking at their freely selected speed (Table 1). There are two possible explanations for this difference. First, measurements of metabolic energy expenditure reported in the literature are for walking with arm swing. Since our model has no arms, it could not benefit from any improvement in metabolic energy consumption that may arise from arm swing. Adding arms to the model would allow us to test the hypothesis that arm swing *decreases* metabolic energy expenditure during gait. Second, it is possible that our calculations do not properly account for the various metabolic processes involved in energy production during muscle contraction. Because our model of muscle energetics is phenomenological, it does not dissociate the various chemical processes that underlie muscle metabolism. As a consequence, some of the terms used in the calculation of total muscle energy production may be either overestimated or underestimated in the model. For example, the ratio of activation heat to total energy produced by all the muscles over one gait cycle was 15 percent in the model (Table 1). In contrast, the results of experiments performed on isolated muscles indicate that the proportion of activation heat is roughly 30 percent [23], although in these experiments the muscles are typically subjected to length and velocity profiles which are quite different from those present during walking. Future studies could be aimed at developing a more accurate model of muscle energetics for incorporation in whole-body models of movement.

It is also important to point out several nonphysiological aspects of the muscle model used in this work. Despite the fact that muscles are comprised of different proportions of fast and slow twitch fibers, we assumed that each muscle in the model had a maximum shortening velocity of ten optimal fiber lengths per second ($10\,l_m^0/s$), which is rather high [15]. One of the goals of our work was to develop a single musculoskeletal model that could be used to simulate a variety of activities. Some activities, like maximum-height jumping, are explosive and require the recruitment of mainly fast-twitch fibers. Walking, on the other hand, is an activity that requires the recruitment of mainly slow-twitch muscle fibers. While it would have been more accurate to separate each muscle excitation signal into a slow and fast twitch component, this was not computationally feasible because it would have meant doubling the number of controls in the model. We were therefore left with having to approximate the summed effect of slow, intermediate, and fast muscle fiber types with a single shortening velocity. Our simulations of maximum-height jumping showed that lower values of maximum shortening velocity (i.e., values less than $10\,l_m^0/s$) caused the model to jump lower than our subjects. Thus, for a general purpose model, we reasoned that it was better to use a value of muscle's maximum shortening velocity that was too high rather than too low.

Another criticism that can be directed at our muscle model is that it is a lumped-parameter model. For example, all sarcomeres within a given muscle are assumed to have the same length, which is known not to be the case [24]. This assumption had observable effects for soleus, a muscle which has relatively short fibers. Using an optimal fiber length of 3 cm for soleus [13] meant that it was not possible to reproduce the broad plantarflexion torque-angle curve that was measured at the ankle for our subjects. To compensate for this limitation, we increased the optimal fiber length of soleus and reduced its maximum isometric strength accordingly.

Owing largely to computational expense, dynamic simulation has not yet found its stride, and researchers in computational biomechanics continue to focus on finding more efficient and fruitful approaches to simulating movement [25–27]. The dynamic optimization solution presented here represents another step toward developing a mathematical representation of the whole body which integrates neural control with muscle physiology and skeletal dynamics. We believe the ability to predict novel movement is particularly important because it offers the possibility of investigating how structure impacts coordination and function. One could, for example, systematically alter the structure of a model, re-solve the problem, and use the predicted changes as a basis for recommending surgical procedures for the correction of gait pathologies or for improving the design of a joint replacement. Unfortunately, despite the great computational power our supercomputers currently possess, we believe this kind of functional analysis is still just beyond our grasp. At the same time, however, we are confident, given the still increasing speeds of computer processors, the growing availability of parallel resources (i.e., the internet), and the potential for improving our computational algorithms, that it is only a matter of time before this kind of functional analysis will become a valuable clinical and engineering tool.

Acknowledgments

This work was supported by the Whitaker Foundation, NASA Grant No. NAG5-2217, the National Aerospace Simulation Program at NASA-Ames Research Center, and the Center for High Performance Computing at The University of Texas at Austin. We thank Prof. Herbert Hatze for reviewing an earlier draft of this paper and for offering many constructive comments on our work.

References

[1] Crowninshield, R. D., and Brand, R. A., 1981, ''A Physiologically Based Criterion of Muscle Force Prediction in Locomotion,'' J. Biomech., **14**, pp. 793–801.
[2] Patriarco, A. B., Mann, R. W., Simon, S. R., and Mansour, J. M., 1981, ''An Evaluation of the Approaches of Optimization Methods in the Prediction of Muscle Forces During Human Gait,'' J. Biomech., **14**, pp. 513–525.
[3] Pedersen, D. R., Brand, R. A., and Davy, D. T., 1997, ''Pelvic Muscle and Acetabular Contact Forces During Gait,'' J. Biomech., **30**, pp. 959–965.
[4] Glitsch, U., and Baumann, W., 1997, ''The Three-Dimensional Determination of Internal Loads in the Lower Extremity,'' J. Biomech., **30**, pp. 1123–1131.
[5] Davy, D. T., and Audu, M. L., 1987, ''A Dynamic Optimization Technique for Predicting Muscle Forces in the Swing Phase of Gait,'' J. Biomech., **20**, pp. 187–201.
[6] Anderson, F. C., and Pandy, M. G., 2001, ''Static and Dynamic Optimization Solutions for Gait Are Practically Equivalent,'' J. Biomech., **34**, pp. 153–161.
[7] Yamaguchi, G. T., and Zajac, F. E., 1990, ''Restoring Unassisted Natural Gait to Paraplegics Via Functional Neuromuscular Stimulation: A Computer Simulation Study,'' IEEE Trans. Biomed. Eng., **37**, pp. 886–902.
[8] Anderson, F. C., Ziegler, J. M., Pandy, M. G., and Whalen, R. T., 1995, ''Application of High-Performance Computing to Numerical Simulation of Human Movement,'' ASME J. Biomech. Eng., **117**, pp. 155–157.
[9] Chow, C. K., and Jacobson, D. H., 1971, ''Studies of Human Locomotion Via Optimal Programming,'' Math. Biosci., **10**, pp. 239–306.
[10] Anderson, F. C., 1999, ''A Dynamic Optimization Solution for a Complete Cycle of Normal Gait,'' Ph.D. thesis, The University of Texas at Austin, Austin, Texas.
[11] Anderson, F. C., and Pandy, M. G., 1999, ''A Dynamic Optimization Solution for Vertical Jumping in Three Dimensions,'' Comput. Meth. Biomech. Biomed. Eng., **2**, pp. 201–231.
[12] McConville, J. T., Clauser, C. E., Churchill, T. D., Cuzzi, J., and Kaleps, I., 1980, ''Anthropometric Relationships of Body and Body Segment Moments of Inertia,'' Technical Report AFAMRL-TR-80-119, Air Force Aerospace Medical Research Laboratory, Wright-Patterson AFB, OH.
[13] Delp, S. L., 1990, ''Surgery Simulation: A Computer Graphics System to Analyze and Design Musculoskeletal Reconstructions of the Lower Limb,'' Ph.D. thesis, Stanford University, Stanford, CA.
[14] Garner, B. A., and Pandy, M. G., 2000, ''The Obstacle-Set Method for Representing Muscle Paths in Musculoskeletal Models,'' Comput. Meth. Biomech. Biomed. Eng., **3**, pp. 1–30.
[15] Zajac, F. E., 1989, ''Muscle and Tendon: Properties, Models, Scaling, and Application to Biomechanics and Motor Control,'' *CRC Critical Reviews in Biomedical Engineering*, J. R. Bourne, ed., CRC Press, Baca Raton, Vol. 19, pp. 359–411.
[16] Ralston, H. J., 1976, ''Energetics of Human Walking,'' in: *Neural Control of Locomotion*, R. M. Herman et al., eds., Plenum Press, New York, pp. 77–98.
[17] Hatze, H., and Buys, J. D., 1977, ''Energy-Optimal Controls in the Mammalian Neuromuscular System,'' Biol. Cybern., **27**, pp. 9–20.
[18] Mommaerts, W. F., 1969, ''Energetics of Muscular Contraction,'' Physiol. Rev., **49**, pp. 427–508.

[19] Pandy, M. G., Anderson, F. C., and Hull, D. G., 1992, ''A Parameter Optimization Approach for the Optimal Control of Large-Scale Musculoskeletal Systems,'' ASME J. Biomech. Eng., **114**, pp. 450–460.
[20] Burdett, R. G., Skrinar, G. S., and Simon, S. R., 1983, ''Comparison of Mechanical Work and Metabolic Energy Consumption During Normal Gait,'' J. Orthop. Res., **1**, pp. 63–72.
[21] Heglund, N. C., and Cavagna, G. A., 1982, ''Mechanical Work, Oxygen Consumption, and Efficiency in Isolated Frog and Rat Muscle,'' Am. J. Physiol., **253**, pp. C22–C29.
[22] Saunders, J. B., Inman, V. T., and Eberhart, H. D., 1953, ''The Major Determinants in Normal and Pathological Gait,'' J. Bone Jt. Surg., Am. Vol., **35-A**, pp. 544–553.
[23] Homsher, E., Mommaerts, W. F. H. M., and Ricchiuti, N. V., 1973, ''Energetics of Shortening Muscles in Twitches and Tetanic Contractions. II. Force-Determined Shortening Heat,'' J. Gen. Physiol., **62**, pp. 677–692.
[24] Huijing, P. A., 1995, ''Parameter Interdependence and Success of Skeletal Muscle Modeling,'' Human Movement Sci., **14**, pp. 443–486.
[25] Taga, G., 1995, ''A Model of the Neuromusculoskeletal System for Human Locomotion: Emergence of Basic Gait,'' Biol. Cybern., **73**, pp. 95–111.
[26] Kaplan, M. L., and Heegaard, J. H., 1999, ''Fast Optimal Control Solution Algorithm for Muscular Activity in Human Locomotion,'' *Proc. 1999 Bioengineering Conference*, V. K. Goel et al., eds., ASME BED-Vol. 42, pp. 413–414.
[27] Pandy, M. G., 2001, ''Computer Modeling and Simulation of Human Movement,'' Ann. Rev. Biomed. Eng., **3**, pp. 245–273.
[28] Rab, G. T., 1994, ''Muscle,'' in: *Human Walking*, J. Rose and J. G. Gamble, eds., Williams and Wilkins, Baltimore, pp. 103–121.
[29] Waters, R. L., and Morris, J. M., 1972, ''Electrical Activity of Muscles of the Trunk During Walking,'' J. Anat., **111**, pp. 191–199.